Natural Hazards (2022) 113:1151–1176
https://doi.org/10.1007/s11069-022-05341-8

ORIGINAL PAPER

# Projected changes in meteorological drought over East Africa inferred from bias-adjusted CMIP6 models

**Brian Ayugi[1,2] · Zablon Weku Shilenje[3,4] · Hassen Babaousmail[5] · Kenny T. C. Lim Kam Sian[5] · Richard Mumo[6] · Victor Nnamdi Dike[7,8] · Vedaste Iyakaremye[2,9] · Abdelghani Chehbouni[10] · Victor Ongoma[10]**

Received: 16 October 2021 / Accepted: 25 March 2022 / Published online: 9 April 2022


## Abstract

The ongoing global warming has caused unprecedented changes in the climate system, leading to an increase in the intensity and frequency of weather and climate extremes. This study uses the sixth phase of Coupled Model Intercomparison Project (CMIP6) data to investigate projected changes in drought events over East Africa (EA) under four Shared Socioeconomic Pathway (SSP) emission scenarios (SSP1-2.6, SSP2-4.5, SSP3-4.0, and SSP5-8.5). The CMIP6 data are bias-corrected using a quantile mapping method, with the Climatic Research Unit's precipitation dataset as reference. Drought is quantified using the standardized precipitation index and different measures of drought are estimated: drought duration, drought frequency, drought severity, and drought intensity. Evaluating the accuracy and reliability of historical data before and after bias correction demonstrates the importance of the approach. The overall distribution after bias correction depicts a close agreement with observation. Moreover, the multi-model ensemble mean demonstrate superiority over individual Global Circulation Models. Projected future changes show enhancement in precipitation over most parts of EA in the far future under different SSP scenarios. However, the arid and semi-arid regions are expected to receive less amount of precipitation, whereas the highlands and lake regions are expected to receive a larger amount of precipitation increase. Furthermore, the dry areas of EA are likely to experience more frequent drought events with longer duration, stronger intensity, and severity in the far future. Overall, this study identifies possible drought hotspots over EA, enabling early preparation for such events.

**Keywords** Precipitation · Drought · Climate change · Quantile mapping · SSP · East Africa

✉ Victor Ongoma
victor.ongoma@gmail.com

Extended author information available on the last page of the article

## 1 Introduction

The earth system continues to witness unprecedented climatic changes (Steffen et al. 2018). An observed increase in the concentration of greenhouse gases (GHGs) in the atmosphere has altered the climate feedback mechanisms (IPCC 2021), posing a significant threat to the survival of both humans and ecosystems. This has led to a "new norm" characterized by the unparalleled occurrence of extreme weather events such as droughts, floods, and heat waves (Eckstein et al. 2019). The impacts of extreme events vary in magnitude, with drought occurrence dominating various economic sectors (IPCC 2014). It is expected to worsen following the intersection of climate change with other environmental and health crises such as the SARS-CoV-2 (COVID-19 novel coronavirus) (Phillips et al. 2020). The damage caused by drought alone is estimated to have affected over 1.5 billion people so far in this century and will likely increase in the future (Jenkins and Warren 2015; Funk et al. 2019; Ukkola et al. 2020). This calls for urgent monitoring of its tendency as a way of identifying hotspots and vulnerable communities for timely interventions and appropriate adaptation strategies (Wilhite et al. 2000; Lloyd-Hughes 2012).

Research shows that the frequency of drought occurrence will increase significantly in the future (Trenberth et al. 2014; IPCC 2014; IPCC 2021), mainly as a consequence of climate change and the rapid rise in population. However, unanimity on the extent of the variation and magnitude of drought is not fully reached (Sheffield et al. 2012). Several climate scenario studies utilize global climate model (GCM) outputs derived from the Coupled Model Intercomparison Project phase three (CMIP3; Meehl et al. 2007; Ostad-Ali-Askari et al. 2019) and/or phase five (CMIP5; Tayler et al. 2012). In general, CMIP5 ensembles depict an increase in the intensity and frequency of droughts globally in the twenty-first century (Sheffield and Wood 2008; Dai 2013; Huang et al. 2016). To illustrate, most climate models highlight a significant increase in drying patterns in central Europe, particularly in Poland (Osuch et al. 2016), western North America (Ahmadalipour et al. 2017; Wei et al. 2019; Zhao et al. 2021), the Mediterranean (Trenberth et al. 2014), the Amazon (Duffy et al. 2015), Africa (Masih et al. 2014; Haile et al. 2020), South Asia (Wang et al. 2018; Zhai et al. 2020), and Australia (van Dijk et al. 2013). Despite the robust projections that have been conducted over different parts of the world using the CMIP datasets, there remain some uncertainties and biases in the model results (Burke and Brown 2008). Such biases cast aspersions on the reliability of the projections based on previous model outputs (Ukkola et al. 2018), thus calling for a concerted effort for improved model parameterization.

The new generation of CMIP outputs (CMIP6; Eyring et al. 2016) provides an opportunity to enhance our understanding of the future climate. Policymakers, among other users of climate information, need timely information that will enable them to address pertinent climate-related issues, especially responses to disasters. Many recent studies have examined drought changes using CMIP6 multi-model ensembles at global and regional scales (Ukkola et al. 2020; Cook et al. 2020; Zhai et al. 2020; Shrestha et al. 2020). For instance, Ukkola et al. (2020) report an increase in drought occurrence by more than 45% worldwide, mainly due to changes in mean precipitation and natural variability. The findings concur with a related study by Cook et al. (2020) that notes a severe drying pattern with an anomalous increase in extreme drought events by up to 300% in some locales. Meanwhile, regional studies demonstrate a concomitant tendency to that of global land area analysis. For example, Zhai et al. (2020) reported a significant increase in drought features over the northwest sub-region of the larger southeast Asia domain using a CMIP6 ensemble. While

conducting drought changes analysis over regions of India using bias-corrected CMIP6 data, Shrestha et al. (2020) observed that multiple severe-to-extreme drought events would intensify during the 2030s in most climate scenarios.

Africa remains one of the most vulnerable continents to drought-related impacts as a result of technological, institutional, and financing constraints (Ahmadalipour et al. 2019; IPCC 2022). With the largest expanse of drylands exceeding the aridity index of 0.05 (Huang et al. 2016), the observed and projected drought intensification will negatively impact nearly all spheres of livelihood. Wei et al. (2019) showed that drier and hyper-arid regions would experience higher warming of 2.4 °C under the worst-case emission scenario (O'Neill et al. 2017). The projected warming will raise the temperature of dryland regions of the Sahara Desert and Southern Africa by 5.6 °C and 1.4°C, respectively, under the Shared Socioeconomic Pathway (SSP) 5–8.5 (Almazouri et al. 2020). The escalation in temperature coupled with declining precipitation over most regions of Africa is likely to exacerbate the occurrence of drought events.

A few CMIP6-based studies (e.g., Cook et al. 2020; Ukkola et al. 2020) have been conducted over Africa's hydroclimatic sub-regions to examine the drought changes. The existing studies over EA focus on precipitation changes owing to the observed decrease in the March to May (MAM) seasonal rainfall (Funk et al. 2014; Ongoma and Chen 2017; Nicholson 2017). The region's most common extreme weather events are droughts and floods (Lukamba 2010; Nkunzimana et al. 2021; Fatahi Nafchi et al. 2022). These events cause losses of lives, disruption of livelihoods, and destruction of property in EA (Otieno and Awange 2006; Lyon and Dewitt 2012; Opiyo et al. 2015), calling for response measures that, often, consume millions of dollars annually (Martey et al. 2020).

The availability of CMIP6 GCMs provides an opportunity to re-examine the future changes in drought events and map out possible drought hotspots over EA. In comparison with the previous generation (i.e., CMIP5, Tayler et al. 2012), CMIP6 includes more comprehensive GCMs with generally more sophisticated physics and higher resolution, which yield a better representation of the observed climate systems (Ayugi et al. 2021a, b, c). Moreover, the SSPs (O`Neill et al. 2017) provides additional descriptions of socioeconomic development, unlike the previous versions of representative concentration pathways (RCPs; Van Vuuren et al. 2011) that only captured the projections of the components of radiative forcing for use for assessment of changes in the climate system. Subsequently, these SSPs were considered and applied in the latest Sixth Assessment Report (AR6; IPCC 2021) to examine how the societal actions will impact the emissions of greenhouse gases (GHGs) and also how climate goals under Paris Agreement will be attained.

Thus, this work employs the latest SSP scenarios under CMIP6 to examine the projected future changes in drought characteristics over East Africa. Notably, the biases reported in the previous versions of the CMIP simulations also exist in the CMIP6 simulations (Abdelmoaty et al. 2021; Tian and Dong 2020). Therefore, bias correction is herein introduced to obtain a reliable future projection of drought characteristics over the region. This information is needed for devising effective adaptation and mitigation strategies in the region that has remained a drought hotspot and vulnerable to its effects (Trisos et al. 2022; Ayugi et al. 2022). This study uses the Standardized Precipitation Index (SPI) to build an accurate drought map for EA. Ukkola et al. (2020) advocated for the use of SPI since other approaches that incorporate potential evapotranspiration (PET) such as Standardized Precipitation Evapotranspiration Index (SPEI) tend to overestimate projected future drought. According to Swann et al. (2016), including PET in the computation of droughts tends to introduce errors by double-counting the effects of surface humidity and temperature on droughts. In a different study, Ntale and Gan (2003) reported that SPI is more suitable for

application over the region, as compared to Palmer drought severity index (PDSI) and the Bhalme–Mooley index (BMI) over East Africa,

This study thus seeks to answer one main question: What is the spatial and temporal extent of projected drought extremes over EA? This information is useful in improving the accuracy and reliability of existing drought early warning systems. The rest of the paper is organized as follows: Sect. 2 describes the physical, climate, and socio-economic outlook of the study area, data used, and the methods while Sect. 3 highlights the key findings and related discussions. Finally, Sect. 4 captures conclusions and recommendations for further studies.

## 2 Study area, data, and methods

### 2.1 Study area

EA lies in the equatorial region, within 28° E–42° E and 12° S–5° N (Fig. 1). In this study, Rwanda and Burundi are regarded as part of Tanzania owing to their relatively small size and having homogenous climate with Tanzania. Other countries in the region considered are Kenya and Uganda. The Great Rift Valley divides the study area into nearly two halves. Others entail Africa's largest lake, Lake Victoria, among other large inland water bodies that partly regulate moisture distribution in the region (Song et al. 2004), as well as being a source of livelihood to the region's population (Ntiba et al. 2001). The region equally has the highest elevation point in Africa with a height of more than 5800 m (Mt. Kilimanjaro),

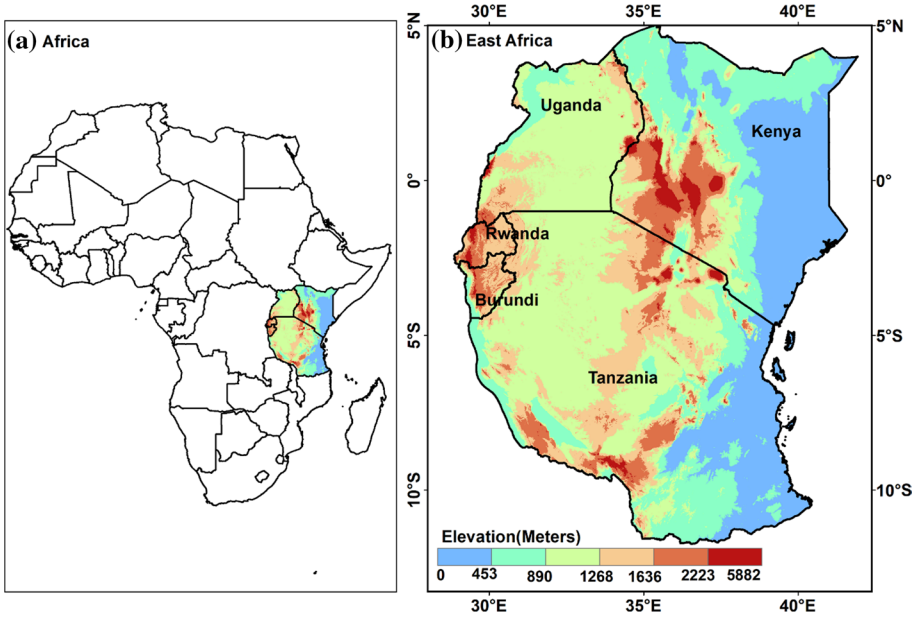


**Fig. 1** Diagrammatic sketch of the African continent and elevation map (m) of East Africa, consisting of three countries: Kenya [35°E–41.5°E, 3°S–4.5°N], Uganda [29°E–5°E, 1.5°S–4°N], and Tanzania [29°E–40°E, 10°S–4°S].

followed by Mt. Kenya (> 5199 m) and Mt. Ruwenzori (> 5109 m). Other features include the largest expanse of Arid and Semi-Arid Lands (ASAL) covering most parts of eastern Kenya, Somalia, and northern Uganda (Camberlin 2018).

The average mean annual precipitation over EA ranges between 800 and 1200 mm, characterized by a high spatio-temporal distribution (Indeje et al. 2001; Ongoma et al. 2018a). This is due to the region's complex topography, water bodies, and maritime influence (Ogwang et al. 2014). Most parts of the region, especially Kenya, the western part of Uganda, and eastern Tanzania, receive a bimodal rainfall distribution during MAM and October–December (OND) (Kabanda and Jury 1999; Ongoma and Chen 2017; Gebrechorkos et al. 2020). The rainfall seasonality is mainly influenced by the movement of the inter-tropical convergence zone (Nicholson 2018). Rainfall interannual variability is also influenced by El Niño and La Niña (El Niño-Southern Oscillation, ENSO) and other factors such as the Quasi-Biennial Oscillation (QBO) and Indian Ocean Dipole (IOD) (Endris et al. 2016). On the other hand, the temperature is generally warm throughout the year, ranging between 19 and 30 °C (Ongoma and Chen 2017; Camberlin 2018; Ayugi and Tan 2019). Generally, the region is classified as tropical savanna climate (Peel et al. 2007). The warmest months across the region are January and February while the coolest month is between June to September (Ongoma and Chen 2017). More details on the area of study can be found in Camberlin (2018).

### 2.2 Datasets

This study utilizes the gridded monthly rainfall data from the University of East Anglia Climatic Research Unit (CRU version TS4.04) spanning 120 years (1901–2020) as observed data. The data have been successfully used in related studies over EA (e.g., Ogwang et al. 2014, 2015; Maidment et al. 2015; Ongoma et al. 2015, 2018b; Sagero et al. 2018; Ayugi et al. 2018). The CRU data are preferred over station data because it has a long time series and is quality controlled. Most weather records over EA are of low quality and have short records, many of which are less than 50 years and exhibit incompleteness, as reported by several studies (e.g., Omondi et al. 2014; Ongoma et al. 2018c). The CRU data are created by interpolating station data on a $0.5° \times 0.5°$ resolution grid (Harris et al. 2014). A detailed description of the CRU version TS4.04 data is provided by Harris et al. (2020). CRU data are preferred over other datasets of similar time length, such as the Global Precipitation Climatology Centre (GPCC) data (Schneider et al. 2015), owing to its higher accuracy in reproducing rainfall over EA (Ayugi et al. 2016; Ongoma and Chen 2017). Many studies recommend the use of datasets with the longest possible time series to examine drought events since most indices detect drought by comparing rainfall over a given period to long term mean (McKee et al. 1993; Wu et al. 2005; Mishra and Sigh 2010).

Further, this study employs a multi-model ensemble (MME) of 16 CMIP6 GCM outputs derived from the first variation run. The datasets are accessed through the Earth Systems Grid Federation (ESGF; https://esgf-node.llnl.gov/search/cmip6/) data replication centers (Eyring et al. 2016). The modelled precipitation for historical and four future scenarios (SSP1-2.6, SSP2-4.5, SSP3-7.0, and SSP5-8.5) are used to estimate drought patterns. The SSP denotes an integrated scenario of possible future climate and societal change, which would be employed to assess topics such as the mitigation and adaptation efforts needed to attain a particular climate outcome (O 'Neill et al. 2016). The historical experiment starts from 1850 to 2014, while projections under the Scenario Model Intercomparison Project (Scenario MIP; O`Neill et al. 2017) run from 2015 to 2100. Table 1 gives the models'

descriptions. The drought index used in the present study is computed from the dataset native resolution and then re-gridded to a consistent spatial resolution of $1° \times 1°$ using a bilinear interpolation technique.

## 2.3 Methods

### 2.3.1 Model bias correction and validation

To improve the reliability of CMIP6 data in projecting the changes in drought properties, the study employs the quantile mapping (QM) based on the gamma distribution bias correction technique (Ines and Hansen 2006; Piani et al. 2010) to minimize the biases reported in recent studies over EA (Akinsanola et al. 2021; Ayugi et al. 2021a; Ngoma et al. 2021). Quantile perturbations adjust the model output values for historical simulation to mimic similar features as the observed data. The same distribution is then enforced on the projection datasets, assuming that the bias is similar in the historical and future periods (Maraun 2013). The Climate Data Bias Corrector developed by Gupta et al. (2019) is used to correct the bias. The empirical cumulative distribution function (ECDF) is used to display the model's performance before and after the QM implementation. The general method of QM is calculated based on Eq. 1 and 2 as follows:

$$F_{m,c}(X_{m,c}) = F_{o,c}(X_{o,c}) \tag{1}$$

$$X_{bc} = F^{-1}_{o,c}\left\{F_{m,p}(x_{m,p})\right\} \tag{2}$$

where $X_{\mathrm{bc}}$ is the corrected variable, and CMIP6 datasets and CRU observation data are denoted by the subscript $m$ and $o$, respectively. $c$ and $p$ represent the calibration and the scenario projected period, respectively. $F_{o,c}$ and $F^{-1}_{0,c}$ are the corresponding empirical cumulative distribution function (*ECDF*) and its inverse in the calibration period. The effectiveness of the technique has been affirmed in previous studies where it was applied on various climatic variables such as precipitation and temperature over different regions (Ayugi et al. 2020a; Tabari et al. 2021; Dike et al. 2022).

### 2.3.2 Drought index and event characteristics

This study examines future meteorological drought evolution over EA using the SPI multiscale drought technique (McKee et al. 1993). The computation of SPI depends mainly on precipitation, based on the assumption that precipitation deficits over varying periods or timescales affect groundwater, reservoir storage, soil moisture, and streamflow (Wu et al. 2005). SPI computes drought events for varying timescales by aggregating the precipitation timescales over the period of interest (i.e., 3 months for SPI-3; 6 months for SPI-6; 9 months for the SPI-9; 12 months for the SPI-12; and 24 months for SPI-24) (McKee et al. 1993).

Subsequently, SPI can be employed to effectively monitor agricultural (SPI-3), hydrological drought (SPI-6), and groundwater (SPI-12 and -24). The drought events over EA are quantified on a three-month timescale (SPI-3) to mirror the seasonal precipitation climatology (MAM and OND) of the study domain. The SPI-3 illustrates the influence of precipitation anomalies on short-term water availability, which is important for rainfed agricultural activities. Compared to other existing drought indices, SPI uses

**Table 1** List of the CMIP6 GCMs used in this study

| S/N | Models | Reporting institutions | Horizontal resolution (lat × lon) |
|---|---|---|---|
| 1 | BCC-CSM2-MR | Beijing climate center (BCC) and China meteorological administration (CMA), China | 1.13° × 1.13° |
| 2 | CanESM5 | Canadian centre for climate modelling and analysis, environment and climate change Canada, Victoria, Canada | 2.81° × 2.81° |
| 3 | CESM2-WACCM | National center for atmospheric research, USA | 1.25° × 0.94° |
| 4 | CMCC-CM2-SR5 | Euro-Mediterranean centre on climate change couple model (CMCC-CM2), Italy | 1.3° × 0.9° |
| 5 | EC-EARTH3 | EC-EARTH consortium, Europe | 0.70° × 0.70° |
| 6 | EC-EARTH3-Veg | EC-EARTH consortium, Europe | 0.70° × 0.70° |
| 7 | FGOALS-g3 | LASG, institute of atmospheric physics, Chinese academy of sciences, China | 2.25° × 2.0° |
| 8 | GFDL-ESM4 | Geophysical fluid dynamics laboratory, USA | 1.25° × 1.00° |
| 9 | HadGEM3-GC31-M | UK met office hadley centre, UK | 1.86° × 1.25° |
| 10 | INM-CM4-8 | Institute for numerical mathematics, Russian academy of science, Moscow, Russia | 2.00° × 1.50° |
| 11 | INM-CM5-0 | Institute for numerical mathematics, Russian academy of science, Russia | 2.00° × 1.50° |
| 12 | KACE-1-0-G | National Institute of Meteorological Sciences/Korea meteorological administration (NIMS-KMA), Republic of Korea | 1.92° × 1.44° |
| 13 | MPI-ESMI-2-HR | Max planck institute, Germany | 0.90° × 1.30° |
| 14 | MRI-ESM2-0 | Meteorological research institute (MRI), Japan | 1.13° × 1.13° |
| 15 | NESM3 | Nanjing University of information science and technology, Nanjing, China | 1.9° × 1.9° |
| 16 | NorESM2-MM | Climate modeling consortium, Norway | 0.9° × 1.25° |

precipitation as an input fit in a gamma distribution. Subsequently, it requires the estimation of gamma distribution parameters such as $\propto$ and $\beta$, which would then transform into a normal distribution as follows (Eq. 3):

$$g(x) = \frac{X^{\propto-1} *_e \frac{-x}{\beta}}{\beta\alpha^{\tau}(\alpha)} \quad for \quad X > 0 \tag{3}$$

where $\propto, \beta, x > 0$ are a shape parameter, a scale parameter, and the precipitation amount, respectively, and $\tau(\propto)$ is the gamma function. The SPI is estimated based on the cumulative probability function as follows (Eq. 4):

$$G(x) = \int_0^x g(x)dx = \frac{1}{\beta^{\alpha}\tau(\alpha)} \int_0^x x^{\alpha-x/\beta_{dx}} \tag{4}$$

where $G(x)$ is cumulative probability of the observed precipitation. If the actual precipitation shows low probability, then the region is under drought prevalence while the reverse probability indicates wet events. Besides, the gamma function is undefined for $x = 0$ and precipitation may have zero values (Gidey et al. 2018). In this study, the cumulative probability function was analyzed as shown in Eq. 5:

$$H(x) = q + (1 - q)G(x) \tag{5}$$

where $q$ is the probability of zero. Estimation of SPI values is derived from a transformation of cumulative probability represented by zero as a mean and variance equal to 1. Subsequently, the long-term mean of historical and projection precipitation data of the study area was computed by summing the whole record and dividing by the number of measurements during the study duration (Eq. 6)

$$\bar{x} = \frac{1}{n} X \sum_{i=0}^{n} x_{i,} \tag{6}$$

where $\bar{x}$ is mean value, $n$ is the number of years (study period), $x_i$ is the value of $i$th timescale being averaged. The standard deviation was also computed to measure the spread of precipitation as follows (Eq. 7):

$$\sigma = \sqrt{\frac{1}{n} \sum_{i=1}^{n} (_{x_i} - \bar{x})^2} \tag{7}$$

where $\sigma$ is the standard deviation, $x_i$ is each value of datasets, $\bar{x}$ is the mean of the data sets, $n$ is the total number of observations and scenario and $\sum$ is the sum of all datasets. A model was then developed to quantify the values of SPI as follows in Table 2 (Eq. 8):

$$SPI = \left(p_i - \overline{p}\right)/\sigma, \tag{8}$$

where $p_i$ is the baseline precipitation value, $\overline{p}$ is the projected mean value, and $\sigma$ is the standard deviation of the projected records.

To investigate the possible changes in drought conditions over the study area, two equal time slices of 30 years are used: the mid-future (2041 – 2070) and the far- future (2071 – 2100) in comparison to the baseline period of 1985 – 2014.

**Table 2** Classification of SPI for drought and wet events (McKee et al. 1993)

| Drought classes | SPI values |
|---|---|
| Extremely wet (EW) | ≥ 2.0 |
| Severe wet (SW) | 1.5–1.99 |
| Moderate wet (MW) | 1.0–1.49 |
| Normal (N) | – 0.99 to 0.99 |
| Moderate dry (MD) | – 1.0 to – 1.49 |
| Severe dry (SD) | – 1.5 to – 1.99 |
| Extreme dry (ED) | ≥ 2.0 |

### 2.3.3 Analysis of drought duration, magnitude, intensity, and frequency

To examine the impact of drought events in the study region, the study considers drought components of drought duration (DD), drought frequency (DF), drought intensity (DI), and drought severity (DS) to detect the possible effects of climate change on drought events in the wake of global warming. The study defines the DS, DI, and DF for dry events over the study domain as given in Eq. 9–11:

(i) Severity is the cumulative sum of the index value based on the duration extent (Eq. 9) as follows:

$$S = \sum_{i=1}^{Duration} Index \tag{9}$$

(ii) The intensity of an event is the severity divided by the duration (Eq. 10). Events that have a shorter duration and higher severity will have large intensities.

$$I = \frac{Severity}{Duration} \tag{10}$$

(iii) Frequency of occurrence $\left(F_s\right)$ is defined in Eq. 11 as follows:

$$F_s = \frac{n_s}{N_s} \times 100\% \tag{11}$$

where $n_s$ is the number of drought events (SPI < – 1 .0), $N_2$ is the total of the months for the study period, and $s$ is a grid cell.

In order to display the changes in drought characteristics listed above, the study employs a boxplot to demonstrate the distribution of DD, DF, DI, and DS over the study area. A box-and-whisker plot is useful in representing the spread and comparison of various drought characteristics. It highlights the distribution of datasets based on five key indicators: minimum value, first quartile (25th percentile), median, third quartile (75th percentile), and maximum value. The interquartile range shows the changes in drought events. This approach is utilized in various studies (e.g., Sheffield et al. 2012; IPCC 2013; Haile et al. 2020).

## 3 Results and discussion

### 3.1 Model correction and validation

The ability of models to simulate observed precipitation is assessed over the study area. The accuracy of future projected changes depends on models' capability to replicate observed values at the historical level (Piani et al. 2010; Tabari et al. 2021). To examine their agreement with observations and the effect of quantile mapping, the GCMs data before (BC) and after correction (AC), together with their MME, are presented in Fig. 2. The results after correction indicate a consistent improvement by all the models and largely agree with the observation. The models before correction over EA (Fig. 2a) remarkably deviate from CRU with an increase in amounts, especially when rainfall exceeds 80 mm. After correction (Fig. 2b), the overall distribution shows a tight agreement with observation. Further statistical analysis of correlation coefficients, RMSEs, and standard deviations, the bias-corrected data show improved skills compared to the original ones (Table S1). For instance, the BC CMIP6-MME shows a correlation coefficient of 0.58, which is improved to 0.8 AC, while the RMSE is reduced from 43.84 (BC) to 39.9 (AC). The standard deviation also denotes an improvement in the individual models and their respective MME after bias correction. The present findings agree with existing studies that highly recommend the correction of inherent GCM biases before employing the data for impact studies (Dosio et al. 2021; Tabari et al. 2021; Ayugi et al. 2021a). In fact, recent studies that employed GCMs in projecting extreme events such as drought, high temperatures, and extreme precipitation equally conducted bias correction before using the model data in examining the projected changes over various locales (Mondal et al. 2021; Iyakaremye et al. 2021; Dosio et al. 2021; Dike et al. 2022), making bias correction powerful mathematical tool for analyzing climate data.

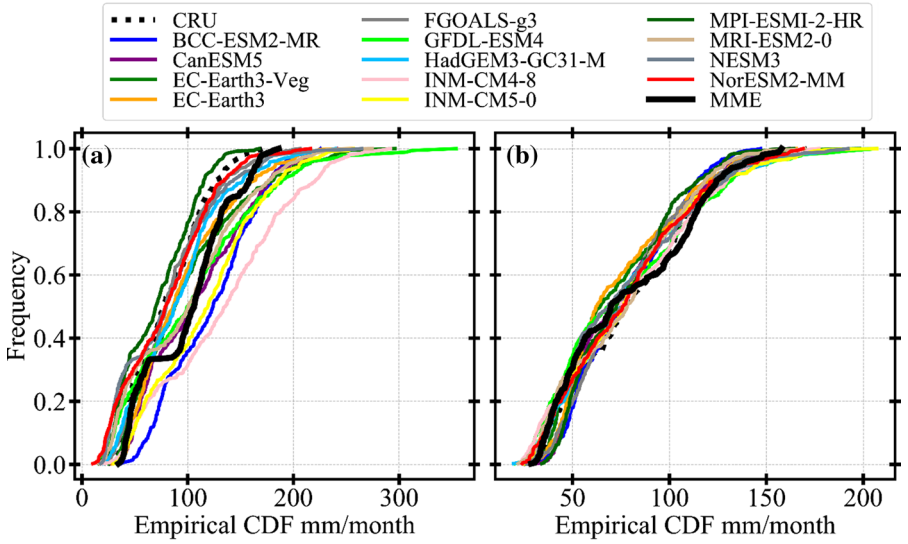


**Fig. 2** Empirical cumulative density function (ECDF; mm/month) of GCMs before **a** and after the bias correction, **b** relative to the precipitation observation (CRU data) over East Africa

### 3.2 Projected change in precipitation

Precipitation is a major factor regulating the occurrence of drought from one region to another (Dai 2018). Other factors include mean surface air temperature, wind speed, humidity, and incoming solar radiation that directly or indirectly affect drought occurrence in terms of enhanced evaporative demand through vapor pressure deficit (IPCC 2014). Thus, it is imperative to understand the projected changes in precipitation to relate the changes to drought events. Figures 3 and 4 show the future temporal and spatial precipitation change over EA relative to the historical period (1995–2014). Generally, all the scenarios depict increasing patterns with differing magnitudes. The SSP5-8.5 scenario shows intensified changes during the far future (15%) relative to the historical period (5%), while minimal changes are predicted to occur under SSP1-2.6 during the mid (3%) and far future (7%) (Fig. 3). Meanwhile, spatial changes in precipitation over EA during the mid and far future depict a homogeneous spread of precipitation with a 100–300% increase under high emission scenarios (Fig. 4d, h). However, negative anomalies are projected to occur over most parts of Kenya and the coastal belt in Tanzania at −40% under SSP1-2.6 during the mid and far future (Fig. 4a, e). Interestingly, a persistent dry anomaly is projected to occur over the coastal belt of Tanzania across all scenarios and timescales, with intense dryness at −60% under SSP1-2.6 and subsequent reduction at −10% under SSP5-8.5 (Fig. 4). Generally, the projected increase in precipitation under a high emission scenario demonstrates the impact of anthropogenic GHG emissions. The results of this study agree with existing literature over EA that demonstrated the pronounced increase in precipitation under high emission scenarios as compared to the low forcing sustainability pathways (Onyutha et al. 2021; Ayugi et al. 2021b; Makula and Zhou 2021). The recently released assessment report of the Inter-governmental Panel on Climate Change Working Group 1 (IPCC 2021) pointed to unprecedented changes that will affect the climate system due to human

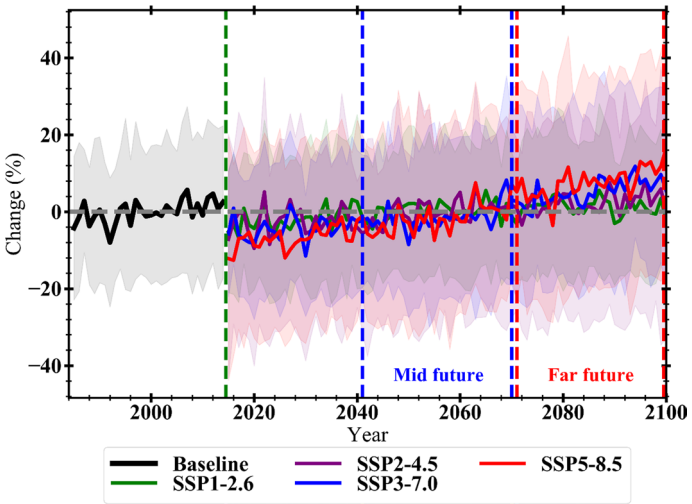


**Fig. 3** Time series of mean precipitation anomaly (%) over East Africa during the historical period (1995–2014), and mid (2041–2070) and far future (2071–2100) under the four SSP scenarios. The black, green, purple, blue, and red lines are the CRU, MME-historical, and SSP1-2.6, SSP2-4.5, SSP3-7.0 and SSP5-8.5 scenarios, respectively. The shadings indicate the GCMs spread. The green dashed line separates the observed period from the projected one

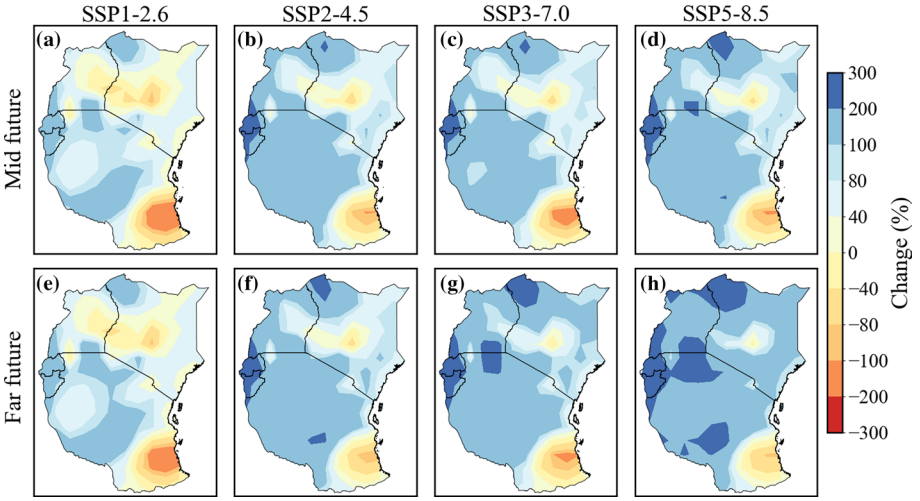


**Fig. 4** Spatial changes in precipitation anomalies (%) for the mid (2041–2070) and far future (2071–2100) periods under SSP1-2.6, SSP2-4.5, SSP3-7.0 and SSP5-8.5 scenarios relative to the baseline period (1985–2014)

influence as a result of GHG emissions. For instance, the report projected an increase or decrease in the frequency and intensity of heavy precipitation over most land areas, leading to more drought or flood events over different regions. It is thus necessary to examine the possible changes in EA's drought characteristics that exhibit high interannual precipitation variability (Ongoma and Chen 2017; Ongoma et al. 2018a, b, c, d; Tan et al. 2020; Ayugi et al. 2021c).

### 3.3 Projected changes in dryness/wetness

To quantify the dryness and/or wetness over EA, the estimated probability distribution functions (PDFs) are shown in Fig. 5. The PDFs are calculated from the regional mean CMIP6 SPI for the baseline period, mid and far future under the selected scenarios. Further, spatial changes in drought patterns based on SPI are presented in Fig. 6. In Fig. 5, there is a clear strong shift indicating notable changes during the far future as compared to mid-future. Strong evidence of change is noted under SSP5-8.5 scenario with a positive anomaly, indicating pluvial anomalies of > 1.5 relative to the baseline period. On the other hand, no remarkable differences were found between scenarios during mid-future compared to the baseline period, except for SSP1-2.6 which depicted a slight positive shift. The rest of the scenarios showed a persistent drying pattern into the mid-future at -1 indicating the occurrence of moderate drought (Fig. 5a). The most striking result to emerge from the analyses is that the wetting situation will be more pronounced as compared to the drought incidences as evident by the magnitude of shifts during both timescales (max SPI value 2 compared to − 1.5). In general, relative to the baseline period, the projected drought changes over EA are characterized by both drying and wetting patterns with average negative SPI anomalies of − 0.06, − 0.03, − 0.13, and − 0.14 for the mid-future and positive SPI of 0.12, 0.20, 0.41, and 0.54 in the far future. Except for SSP1-2.6 (Fig. 5a), the PDFs of SSP2-4.5, SSP3-7.0, and SSP5-8.5 show left-skewness during the mid-future, while this

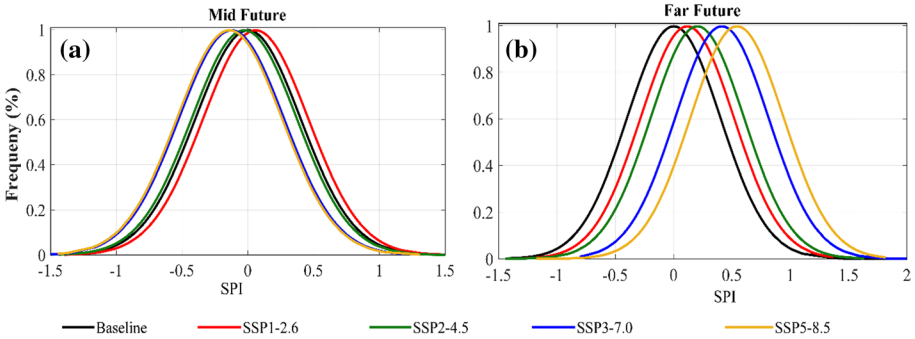


**Fig. 5** PDFs of regional SPI during the **a** mid-future (2041 – 2070) and **b** far future (2071–2100) under SSP1-2.6 (red), SSP2-4.5 (green), SSP3-7.0 (blue), and SSP5-8.5 (orange) scenarios. The baseline period (1985–2014) is plotted in black

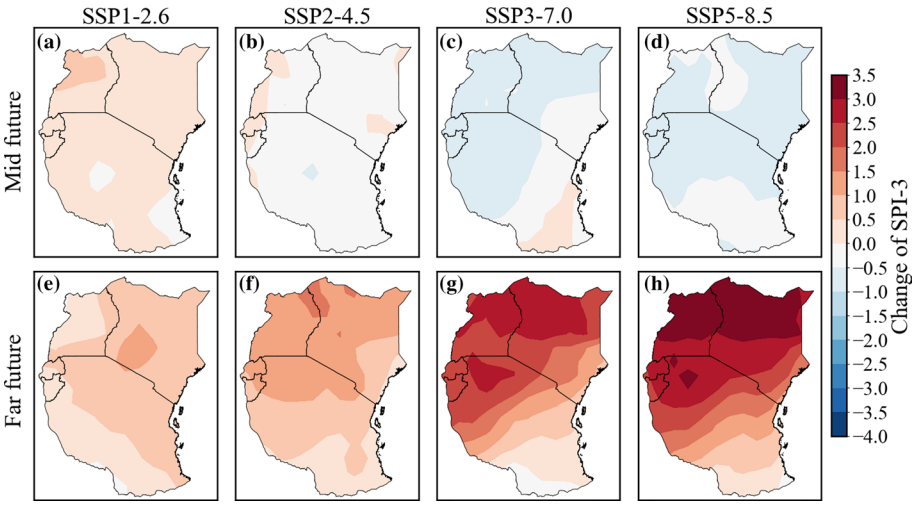


**Fig. 6** Projected change in SPI-3 for mid (2041–2070) and far future (2071 – 2100) under **a**, **e** SSP1-2.6, **b**, **f** SSP2-4.5, (c, g) SSP3-7.0, and **d**, **h** SSP5-8.5 scenarios relative to the baseline period (1985–2014)

phenomenon is expected to lapse into a distinct wetting trend in the far future as portrayed by the right-skewed PDFs (Fig. 5b).

Further analysis to examine spatial changes in drought distribution based on SPI-3 for mid (2041–2070) and far future (2071–2100) under varying scenarios of SSP1-2.6, SSP2-4.5, SSP3-7.0, and SSP5-8.5 scenarios relative to the baseline period (1985 – 2014) are presented in Fig. 6. Similar to the temporal changes as evidenced by PDFs, the spatial distribution of SPI anomaly reveals noteworthy drought (wetness) events during the mid-future (far future) under the SSP3-7.0 and SSP5-8.5 scenarios (Fig. 6). It is clear from the analysis that a uniform wetting pattern will occur over the entire domain during far future ender SSP5-8.5 with strong positive change projected over regions across the north of the equator (Fig. 6h). Strong evidence of severe drought events (SPI = – 1.5) is projected across the entire domain under SSP3-7.0 and SSP5-8.5 during the mid-century (Fig. 6c, d).

Meanwhile, reverse patterns of extreme wetness events of 2.0 to 2.5 are observed toward the end of the twenty-first century (Fig. 6g, h). Obviously, the difference in dryness and wetness is high in the far future and relatively low in the near future.

Taken together, these results suggest that there is an association between the change of drought/flood and the warming levels. Under a high emission scenario, the region will likely experience more extreme precipitation events as compared to the dry anomaly. The results agree with the recent Sixth Assessment Report (IPCC 2021), which noted a projected increase in frequency and intensity of extreme wet events due to human-induced greenhouse gas emission. The persistent dry anomaly during the mid-future indicates evidence of persistent drying patterns that were first detected in 1999 as a result of changes in sea surface temperatures, predominantly in the tropical Pacific basin (Lyon and DeWitt 2012). Conversely, the strong shift from drought to wet events during far future could be mainly attributed to increased moisture in the atmosphere following the Clausius–Clapeyron relationship of the water holding capacity of air which increases by about 7% per 1 °C warming (Trenberth 2011).

### 3.4 Projected changes in drought event characteristics

The absolute spatial changes of drought characteristics during the mid and far future, relative to the baseline period, are shown in Figs. 7, 8, 9, 10. To quantify the changes of drought characteristics, the box plots of regional drought characteristics under the four selected scenarios are shown in Fig. 11. Drought duration is defined as the number of months under drought conditions. The spatial variance and temporal distribution of drought duration are given in Fig. 7a–h and Fig. 11a. The analysis for SPI was derived from an ensemble of 16 bias-corrected GCMs simulations over EA. Units for the DD reflected are based on the number of months/periods in which drought occurrence took place at a

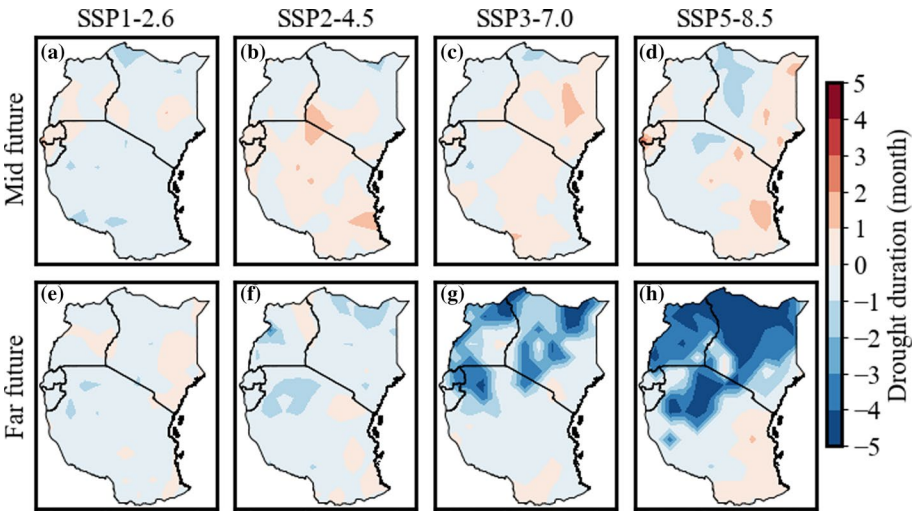


**Fig. 7** Spatial changes in mean drought duration (DD) for the mid-future (2041–2070) and far future (2071–2100) under SSP1-2.6 (first column), SSP2-4.5 (second column), SSP3-7.0 (third column) and SSP5-8.5 (fourth column) relative to the baseline period (1985–2014) over East Africa

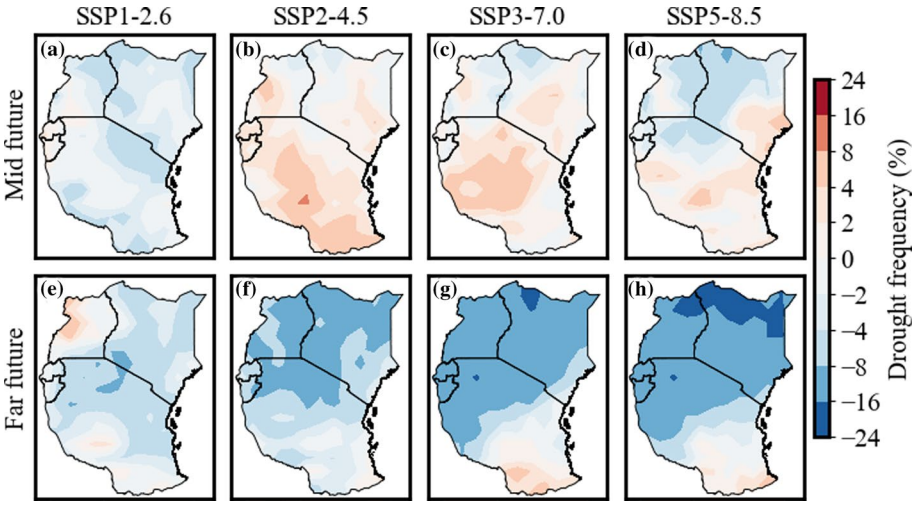


**Fig. 8** Same as Fig. 7, but for drought frequency (DF)

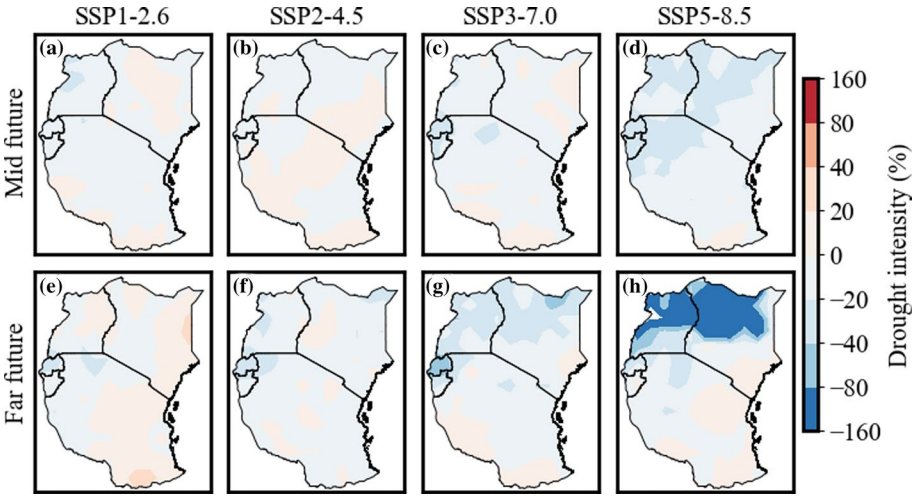


**Fig. 9** Same as Fig. 7, but for mean drought intensity

particular region. Relative to the baseline period, most areas under the four scenarios are projected to experience drought duration in the mid-future while wetting patterns are projected in the far future over EA (Fig. 7). For instance, drought duration for SPI-3 under the most scenario for mid-future (Fig. 7a–d) shows varying patterns of drought changes with regions along the northeast and southeast, stretching toward the coastal belt likely to experience a higher number of months affected by DD as compared to other parts of the study area. The mean drought duration in EA is projected to occur for 3.6, 3.62, 3.8, and 3.85 months under SSP1-2.6, SSP2-4.5, SSP3-7.0, and SSP5-8.5 scenarios, respectively, during the mid-future (Fig. 11a). Mid-future shows the lowest occurrence of DD, except

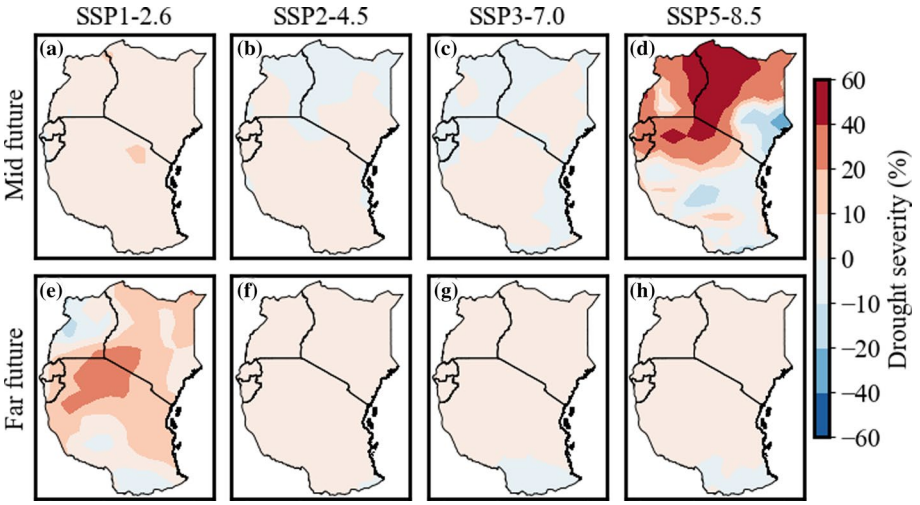


**Fig. 10** Same as Fig. 6, but for mean drought severity (DS)

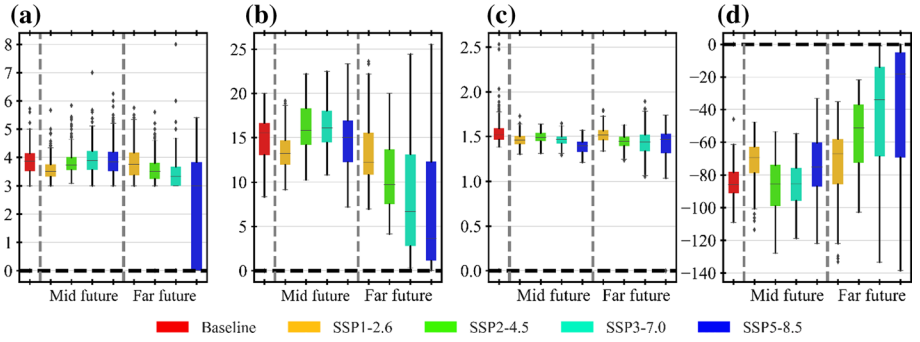


**Fig. 11** Boxplot of drought characteristics during the baseline period, mid-future (2041–2070) and far-future (2071–2100) under four selected scenarios over East Africa. **a** DD, **b** DF, **c** DI and **d** DS. The boxes show the interquartile range, the horizontal lines represent the median and the whiskers show the maximum/minimum value of the lower/upper quartile. The dots are outliers

under the high emission scenario that shows the likely occurrence of longer drought duration. The emission effect from SSP1-2.6 on DD is not evident in the mid-future (Fig. 7a–d) but distinct in the far future (Fig. 7e–h). Interestingly, DD shows a reduction in occurrence toward the far-century (2071–2100), except in the southern belt, and far-end northeastern sides that continue to exhibit occurrence of DD (1–2 months). The locations along eastern sides stretching to the southern belt of the study area are mostly characterized by bare ASALs. Climatic characteristics of such region are predominantly dry with below normal rainfall experienced, leading to increased evapotranspiration which is induced by enhanced radiation, higher wind speed, and vapor pressure deficit, mostly linked to a higher temperature and low relative humidity. Interestingly, locations suited along the western sides and northwest will likely experience fewer months of moderate drought duration. These locations have large water bodies and high elevations coupled with dense vegetations. A recent study (Haile et al. 2020) established that the wetting/drying patterns are directly linked to

the widely known concept of 'dry gets drier and wet gets wetter' paradigm. This pattern is mainly associated with the P and PET which are the main variables in the calculation of the drought index. These are further associated with the water balance (P-PET) estimations where humid regions hold wet with positive P-PET value while arid regions result in deficit/negative P-PET.

The changes in DD during the far future under SSP5-8.5 over the study area which indicate the reduction in drought occurrence toward the end of the century tend to follow the projected trends of precipitation patterns that show a significant increase in future under the scenarios over the study domain, most especially under higher emission scenarios (Shongwe et al. 2011; Tierney et al. 2015; Ongoma et al. 2018a; Ayugi et al. 2021a, b, c). The projected increase in precipitation signifies high pluvial likelihood as compared to drought incidences. The flooding is likely to have an impact on disaster management programs due to infrastructural loss. New emerging challenges will arise due to the coupling scenarios where the projected surface temperature anomalies show a positive trajectory across the globe and over the study region (Ongoma et al. 2018a). The study area is likely to encounter serious problems associated with health as a result of vector-borne disease and other pestilences.

Figures 8 and 11b present spatially averaged drought frequency over EA that amounts to 15% during the baseline period, 13% (average value from all scenarios) in the mid-future (Figs. 8a–d and 11b), and 9% in the far future (Figs. 8e–h and 11b). From the SPI-3 results for SSP2-4.5 and SSP3-7.0 scenarios (Fig. 7b, c), it is evident that the study domain will likely experience an intensification and a more frequent occurrence of extreme incidences during the mid-future time slice than during the baseline period. This suggests that EA may experience more drought frequency in the mid future. However, late century projections show that the study area is likely to experience a sharp reduction in severe and extreme occurrence to more of moderate drought frequency from 14% under the low-emission scenario (SSP1-2.6) to 3% under the high-emission scenario (SSP5-8.5). Late-century drought projections under medium stabilization without shoot show occurrence of moderate to severe events and likely occurrence of high intense occurrence of an extreme event. The causes of extreme drought are still unknown and likely to be revealed in further studies. This implies the possibility of a higher DF during the mid future and a lower DF in the far future. This is consistent with the dryness changes shown in Figs. 5 and 6. Interestingly, DF in the far future is projected to increase considerably (Fig. 8e–h), particularly under the average no policy (SSP3-7.0) and worst case no policy (SSP5-8.5) (Fig. 8g, h) along the coastal belt of the Tanzanian region. The regions dominated by dry changes (e.g., northern Kenya, the northern parts of Uganda, and northern tips of Tanzania, as shown in Fig. 6) tend to experience more drought events in the mid future under the four scenarios (Fig. 8a–d). For example, relative to the baseline period with an average drought frequency, Kenya, Uganda, Rwanda, and Burundi are projected to experience more drought events in the mid future (2%, 4%, and 8%) under SSP2-4.5, SSP3-7.0, and SSP5-8.5 scenarios (Fig. 8b, c, d), respectively.

The examination of DI, computed as the ratio between DS and DD, is presented in Figs. 9 and 11c. The DI is used to measure the overall intensity of drought events. For example, drought events of similar severity may have very different intensities if their durations are different. The mean values of DI are calculated for the historical and future periods under the different scenarios. The absolute changes in DI during the mid and far future are shown in Fig. 9a–h, and the regional DI statistics are given in Fig. 11c. Generally, relative to the baseline period, EA's DI preserves similar or becomes lower in the far future and becomes higher in the mid future under the different scenarios. DI will likely impact

the northeastern parts of Kenya and Uganda during the mid future under SSP3-7.0 and SSP5-8.5 (Fig. 9c, d). In the mid future, relative to the baseline period, EA will experience higher DI than the baseline period at 10, 22, 21, and 25% under SSP1-2.6, SSP2-4.5, SSP3-7.0, and SSP5-8.5, respectively. Similarly, in the far future, the region is likely to experience DI at 14%, 10%, 8%, and 5% under SSP1-2.6, SSP2-4.5, SSP3-7.0, and SSP5-8.5, respectively.

Lastly, the study assesses the changes in DS, which is defined as the cumulated SPI value during the drought event and is used to measure drought magnitude. The larger the DS value, the more severe the drought. The absolute change in mean drought severity is calculated for each grid in the mid and far future under the four future scenarios (Fig. 10a–h). In addition, the statistics of DS over EA are also shown in Fig. 11d. In general, EA is projected to experience a more severe drought during the mid and far future under the different scenarios. As expected, DS increases much more in the mid future than in the far future, partly contributed to by the great increase in DD as presented in Fig. 7. The coastal region and parts of Tanzania are projected to experience less severe droughts in the far future under SSP5-8.5 scenarios (Fig. 10d). The effect of emission concentration is not apparent in the far future in most regions. In western Kenya and north parts of Tanzania, there is an interesting higher DS for the low emission concentration (Fig. 10e), while in the far future, the emission concentration effects on DS are less significant over the entire region (Fig. 10f–h).

The results agree with previous studies conducted over the region based on the Representative Concentration Pathways (RCPs) scenario derived from CMIP5 data and demonstrated an increase in wetness and dryness during the far future (Tan et al. 2020; Spinoni et al. 2020). For instance, related studies (e.g., Nguvava et al. 2019; Haile et al. 2020) showed an increase in drought events, mainly attributed to increased evaporation from higher temperatures. The studies mentioned above were mainly based on the Standardized Precipitation Evapotranspiration Index (SPEI) which accounts for both precipitation and PET. Supportably, Joeng et al. (2014) affirmed that the observed and projected drought extremes are mainly driven by an increase in mean surface temperature and PET. In fact, recent studies based on CMIP6 models (e.g., Almazroui et al. 2020; Ayugi et al. 2021c; Iyakaremye et al. 2021) have all pointed out a steady increase in mean and extreme temperature properties over EA comparative to other sub-regions of the continent. For instance, Almazroui et al. (2020) stated that the increasing trend in temperature over EA under SSP1-2.6, SSP2-4.5, and SSP5-8.5 is projected to be 0.03, 0.22, and 0.49 °C decade$^{-1}$, respectively.

However, other researchers have remarked that the more pronounced drought events projected at a regional level are mainly due to uncoupled modelling approaches that largely overestimate regional drought events due to wrong assumptions under increasing $CO_2$ emissions (Swann et al. 2016; Yang et al. 2019). Overall, the projected drought changes over EA follow changes in emissions and different periods. The mid future shows persistent drought events under medium forcing middle-of-the-road pathways (+7.0 W m$^{-2}$) and high-end forcing pathways (+8.5 W m$^{-2}$), reflecting a sustained pattern observed since 1992, following intense warming that occurred along the Western Indian Ocean (Lyon and DeWitt 2012; Liebmann et al. 2014) and SST variations over the Indo-Pacific associated with the Walker circulation (Hua et al. 2016) over EA. In contrast, during the far future, the region will likely experience more wetness under SSP3-7.0 and SSP5-8.5 as compared to the low emission scenario of SSP1-2.6 or under low forcing sustainability pathways of SSP2-4.5. The results reaffirm the conclusions of the IPCC (2021) that reported with high confidence the influence of humans on climate, causing climate change.

## 4 Conclusion

This study employs bias-corrected data derived from CMIP6 GCMs to assess the future changes in meteorological drought over EA. Four scenarios (SSP1-2.6, SSP2-4.5, SSP3-7.0, and SSP5-8.5), representing different ranges of future GHGs emissions and land use are used to project changes in drought during two time slices: mid future (2041–2070) and far future (2071–2100), relative to a baseline period (1985–2014). The CMIP6 GCMs' ability to capture the multi-year annual precipitation spatial patterns improves when the models are subjected to quantile gamma mapping. The overall distribution shows a tight agreement with observation. The MME shows superiority over individual GCMs. Also, the BC (AC) CMIP6 MME shows a correlation coefficient of 0.58 (0.8). The RMSE is equally reduced from 43.84 before correction to 39.9 after bias correction. The downscaled GCMs and their ensembles can be used for drought monitoring over EA. Our finding demonstrats that large parts of EA are expected to get more precipitation in the future under different scenarios. However, the spatial heterogeneity of the increase in precipitation magnitude is high. In general, dry regions are expected to receive less precipitation increase, whereas highlands and lake regions are expected to receive a larger amount of precipitation. In the late twenty-first century (2071–2100), the increase in precipitation is projected to be much higher than during the mid future. Generally, relative to the baseline period, the projected drought changes over EA are characterized by both drying and wetting patterns with average negative SPI of −0.06, −0.03, −0.13, and −0.14 for the mid future and positive SPI of 0.12, 0.20, 0.41, and 0.54 in the far future under SSP1-2.6, SSP2-4.5, SSP3-7.0, and SSP5-8.5, respectively. From the low to high emission scenarios, the drying pattern is observed in the mid future, while this phenomenon is expected to lapse into a distinct wetting trend in the far future. Obviously, the difference in dryness and wetness is larger in the far future and relatively smaller in the mid future. Lastly, projected changes in drought event characteristics considering the duration, intensity, frequency, and severity are examined on how they will evolve over the study domain during the mid and far future under varying climate change scenarios. Overall, drought events are likely to occur more frequently over the dry regions (ASAL) of EA with longer durations, and more significant severity and intensity in the far future under the four different scenarios. Precipitation and SPI-3 also project a similar trend in the far future. For instance, the mean drought duration in EA is projected to occur for 3.6, 3.62, 3.8, and 3.85 months under SSP1-2.6, SSP2-4.5, SSP3-7.0, and SSP5-8.5 scenarios, respectively, during the mid future. Considering DF, relative to the baseline period, the region will likely experience more drought events in the mid future (2%, 4%, and 8%) under SSP2-4.5, SSP3-7.0, and SSP5-8.5 scenarios, respectively. DI will likely impact the northeastern parts of Kenya and Uganda during the mid future under SSP3-7.0 and SSP5-8.5. In the mid future, relative to the baseline period, EA will experience higher DI than the baseline period at 10, 22, 21, and 25% under SSP1-2.6, SSP2-4.5, SSP3-7.0, and SSP5-8.5, respectively. Similarly, in the far future, the region is likely to experience DI at 14%, 10%, 8%, and 5% under SSP1-2.6, SSP2-4.5, SSP3-7.0, and SSP5-8.5, respectively. The findings of this study call for further quantification of drought changes, particularly over dry regions of EA under different warming scenarios of 1.5, 2.0, 3.0, and 4.0 °C. The expected population exposure should also be investigated. This will aid in developing effective short- and long-term mitigation and adaptation strategies against drought events.

**Supplementary Information** The online version contains supplementary material available at https://doi.org/10.1007/s11069-022-05341-8.

**Acknowledgements** The authors appreciate WCRP-WGCM for making the latest CMIP6 outputs publicly available.

**Author contributions** The following are individual contributions: BA, ZWS, AC, VO contributed to conceptualization. BA, AC and VO involved in formal writing and original draft preparation. KTCLKS, VND, ZWS, and HB contributed to data curation, methodology, and visualization. RM, KTCLKS, ZWS and VO involved in writing—review and editing, and investigation. VO, ZWS, and VND contributed to validation.

**Funding** The authors acknowledge the infrastructural support provided by Nanjing University of Information Science and Technology.

**Data availability** The CMIP6 data used in this study can be accessed at no cost from the Earth System Federation portal at https://esgf-node.llnl.gov/search/cmip6. Precipitation data from the Climatic Research Unit (CRU version TS4.04) are also freely available at https://crudata.uea.ac.uk/cru/data/hrg/cru_ts_4.04/.

**Code availability** The data analysis codes are available from B.A. and H.B., and can be shared on request.

## Declarations

**Conflict of interest** All authors declare that they have no conflict of interest.

**Consent for publication** Consents for publication from all the co-authors are received.

## References

Abdelmoaty HM, Papalexiou SM, Rajulapati CR, AghaKouchak A (2021) Biases beyond the mean in CMIP6 extreme precipitation: a global investigation. Earth's Future 9(10):e2021EF002196. https://doi.org/10.1029/2021EF002196

Ahmadalipour A, Moradkhani H, Svoboda M (2017) Centennial drought outlook over the CONUS using NASA-NEX downscaled climate ensemble. Int J Climatol 37:2477–2491. https://doi.org/10.1002/joc.4859

Ahmadalipour A, Moradkhani H, Castelletti A, Magliocca N (2019) Future drought risk in Africa: integrating vulnerability, climate change, and population growth. Sci Total Environ 662:672–686. https://doi.org/10.1016/j.scitotenv.2019.01.278

Akinsanola AA, Ongoma V, Kooperman GJ (2021) Evaluation of CMIP6 models in simulating the statistics of extreme precipitation over Eastern Africa. Atmos Res 254:105509. https://doi.org/10.1016/j.atmosres.2021.105509

Almazroui M, Saeed F, Saeed S, Islam MN, Ismail M, Klutse NAB, Siddiqui MH (2020) Projected change in temperature and precipitation over Africa from CMIP6. Earth Syst Environ 4:455–475. https://doi.org/10.1007/s41748-020-00161-x

Ayugi BO, Tan G (2019) Recent trends of surface air temperatures over Kenya from 1971 to 2010. Meteorol Atmos Phys 131:1401–1413. https://doi.org/10.1007/s00703-018-0644-z

Ayugi BO, Wang W, Chepkemoi D (2016) Analysis of spatial and temporal patterns of rainfall variations over Kenya. Environ Earth Sci 6:69–83

Ayugi BO, Tan G, Ongoma V, Mafuru KB (2018) Circulations associated with variations in boreal spring rainfall over Kenya. Earth Syst Environ 2:421–434. https://doi.org/10.1007/s41748-018-0074-6

Ayugi B, Jiang Z, Zhu H, Ngoma H, Babaousmail H, Karim R, Dike V (2021a) Comparison of CMIP6 and CMIP5 models in simulating mean and extreme precipitation over East Africa. Int J Climatol 41:6474–6496. https://doi.org/10.1002/joc.7207

Ayugi B, Dike V, Ngoma H, Babaousmail H, Mumo R, Ongoma V (2021b) Future changes in precipitation extremes over East Africa based on CMIP6 models. Water 13(17):2358. https://doi.org/10.3390/w13172358

Ayugi B, Ngoma H, Babaousmail H et al (2021c) Evaluation and projection of mean surface temperature using CMIP6 models over East Africa. J Afr Earth Sci 181:104226. https://doi.org/10.1016/j.jafrearsci.2021.104226

Ayugi B, Eresanya E, Onyango AO et al (2022) Review of meteorological drought in Africa: historical trends, impacts, mitigation measures, and prospects. Pure Appl Geophys. https://doi.org/10.1007/s00024-022-02988-z

Ayugi B, Tan G, Ruoyun N, Babaousmail H, Ojara M, Wido H, Mumo L, Ngoma NH, Nooni IK, Ongoma V (2020) Quantile mapping bias correction on rossby centre regional climate models for precipitation analysis over Kenya, East Africa. Water 12(3):801. https://doi.org/10.3390/w12030801

Burke EJ, Brown SJ (2008) Evaluating uncertainties in the projection of future drought. J Hydrometeorol 9:292–299. https://doi.org/10.1175/2007JHM929.1

Camberlin P (2018) Climate of Eastern Africa. In: Camberlin Pierre (ed) Oxford research encyclopedia of climate science. Oxford University Press. https://doi.org/10.1093/acrefore/9780190228620.013.512

Cook BI, Mankin JS, Marvel K, Williams AP, Smerdon JE, Anchukaitis KJ (2020) Twenty-first century drought projections in the CMIP6 forcing scenarios. Earth's Future. https://doi.org/10.1029/2019EF001461

Dai A (2013) Increasing drought under global warming in observations and models. Nat Clim Chang 3:52–58. https://doi.org/10.1038/nclimate1633

Dai A, Zhao T, Chen J (2018) Climate change and drought: a precipitation and evaporation perspective. Curr Clim Chang Rep 4:301–312. https://doi.org/10.1007/s40641-018-0101-6

Dike VN, Lin Z, Kece F, Langendijk GS, Nath D (2022) Evaluation and multi-model projection of seasonal precipitation extremes over Central Asia based on CMIP6 simulations. Int J Climatol (in press)

Dosio A, Jury MW, Almazroui M, Ashfaq M et al (2021) Projected future daily characteristics of African precipitation based on global (CMIP5, CMIP6) and regional (CORDEX, CORDEX-CORE) climate models. Clim Dyn 57:3135–3158. https://doi.org/10.1007/s00382-021-05859-w

Duffy PB, Brando P, Asner GP, Field CB (2015) Projections of future meteorological drought and wet periods in the Amazon. Proc Natl Acad Sci 112(43):13172–13177. https://doi.org/10.1073/pnas.1421010112

Eckstein D, Künzel V, Schäfer L, Winges M (2019) Global climate risk index 2020. Briefing Paper. Germanwatch e.V. Accessed 20, Sep 2021 https://germanwatch.org/sites/germanwatch.org/files/20-2-01e%20Global%20Climate%20Risk%20Index%202020_10.pdf

Endris HS, Lennard C, Hewitson B, Dosio A, Nikulin G, Panitz H-J (2016) Teleconnection responses in multi-GCM driven CORDEX RCMs over Eastern Africa. Clim Dyn 46:2821–2846. https://doi.org/10.1007/s00382-015-2734-7

Eyring V, Bony S, Meehl GA, Senior CA, Stevens B, Stouffer RJ, Taylor KE (2016) Overview of the Coupled Model Intercomparison Project Phase 6 (CMIP6) experimental design and organization. Geosci Model Dev 9:1937–1958. https://doi.org/10.5194/gmd-9-1937-2016

Fattahi Nafchi R, Raeisi Vanani H, Noori PK et al (2022) Investigation on the effect of inclined crest step pool on scouring protection in erodible river beds. Nat Hazards 110:1495–1505. https://doi.org/10.1007/s11069-021-04999-w

Funk C, Hoell A, Shukla S, Bladé I, Liebmann B, Roberts JB, Robertson FR, Husak G (2014) Predicting East African spring droughts using Pacific and Indian Ocean sea surface temperature indices. Hydrol Earth Syst Sci 18:4965–4978. https://doi.org/10.5194/hess-18-4965-2014

Funk C, Shukla S, Thiaw WM et al (2019) Recognizing the famine early warning systems network: over 30 years of drought early warning science advances and partnerships promoting global food security. Bull Am Meteorol Soc 100:1011–1027. https://doi.org/10.1175/BAMS-D-17-0233.1

Gebrechorkos SH, Hülsmann S, Bernhofer C (2020) Analysis of climate variability and droughts in East Africa using high-resolution climate data products. Glob Planet Change 186:103130. https://doi.org/10.1016/j.gloplacha.2020.103130

Gidey E, Dikinya O, Sebego R et al (2018) Predictions of future meteorological drought hazard (~2070) under the representative concentration path (RCP) 4.5 climate change scenarios in Raya. Northern Ethiopia Model Earth Syst Environ 4:475–488. https://doi.org/10.1007/s40808-018-0453-x

Gupta R, Bhattarai R, Mishra A (2019) Development of climate data bias corrector (CDBC) tool and its application over the agro-ecological zones of India. Water 11(5):1102. https://doi.org/10.3390/w11051102

Haile GG, Tang Q, Hosseini-Moghari SM et al (2020) Projected Impacts of Climate Change on Drought Patterns over East Africa. Earth's Future 8(7):e2020EF001502. https://doi.org/10.1029/2020EF001502

Harris I, Jones PD, Osborn TJ, Lister DH (2014) Updated high-resolution grids of monthly climatic observations–the CRU TS3. 10 Dataset. Int J Climatol 34:623–642. https://doi.org/10.1038/s41597-020-0453-3

Harris IC, Osborn TJ, Jones P, Lister D (2020) Version 4 of the CRU TS monthly high-resolution gridded multivariate climate dataset. Sci Data 7:109. https://doi.org/10.1002/joc.3711

Hua W, Zhou L, Chen H, Nicholson SE, Raghavendra A, Jiang Y (2016) Possible causes of the Central Equatorial African long-term drought. Environ Res Lett 11(12):124002. https://doi.org/10.1088/1748-9326/11/12/124002

Huang J, Yu H, Guan X, Wang G, Guo R (2016) Accelerated dryland expansion under climate change. Nat Clim Chang 6:166–171. https://doi.org/10.1038/nclimate2837

Il JD, Sushama L, Khaliq MN (2014) The role of temperature in drought projections over North America. Clim Change 127:289–303. https://doi.org/10.1007/s10584-014-1248-3

Indeje M, Semazzi FHM, Xie L, Ogallo LJ (2001) Mechanistic model simulations of the East African climate using NCAR regional climate model: influence of large-scale orography on the Turkana Low-Level Jet. J Clim 14:2710–2724. https://doi.org/10.1175/1520-0442(2001)014%3c2710:MMSOTE%3e2.0.CO;2

Ines AVM, Hansen JW (2006) Bias correction of daily GCM rainfall for crop simulation studies. Agric Meteorol 138:44–53. https://doi.org/10.1016/j.agrformet.2006.03.009

IPCC (2013) Climate change 2013: the physical science basis. Contribution of working group I to the fifth assessment report of the intergovernmental panel on climate change. In: Stocker TF, Qin D, Plattner GK, Tignor M, Allen SK, Boschung J, Nauels A, Xia Y, Bex V, Midgley PM (eds) Cambridge University Press

IPCC (2014) Summary for policymakers, Climate Change 2014: Impacts, Adaptation, and Vulnerability, Contribution of Working Group II to the Fifth Assessment Report of the Intergovernmental Panel on Climate Change. In: Barros VR, Dokken DJ, Mach KJ, Mastrandrea MD, Bilir TE, Chatterjee M, Ebi KL, Estrada YO, Genova RC, Girma B, Kissel ES, Levy AN, MacCracken S, Mastrandrea PR, White LL (eds) Field CB. Cambridge University Press, Cambridge

IPCC (2021) The Physical science basis. Contribution of working group I to the sixth assessment report of the intergovernmental panel on climate change. In: Zhai P, Pirani A, Connors SL, Péan C, Berger S, Caud N, Chen Y, Goldfarb L, Gomis MI, Huang M, Leitzell K, Lonnoy E, Matthews JBR, Maycock TK, Waterfield T, Yelekçi O, Yu R, Zhou B (eds) Masson-Delmotte V. Cambridge University Press, Cambridge

IPCC (2022) Climate change 2022: impacts, adaptation, and vulnerability contribution of working group II to the sixth assessment report of the intergovernmental panel on climate change. In: Pörtner H-O, Roberts DC, Tignor M, Poloczanska ES, Mintenbeck K, Alegría A, Craig M, Langsdorf S, Löschke S, Möller V, Okem A, Rama B (eds) Cambridge University Press. In Press

Iyakaremye V, Zeng G, Yang X, Zhang G, Ullah I, Gahigi A, Vuguziga F, Asfaw TG, Ayugi B (2021) Increased high-temperature extremes and associated population exposure in Africa by the mid-21st century. Sci Total Environ 790:148162. https://doi.org/10.1016/j.scitotenv.2021.148162

Jenkins K, Warren R (2015) Quantifying the impact of climate change on drought regimes using the Standardised Precipitation Index. Theor Appl Climatol 120:41–54. https://doi.org/10.1007/s00704-014-1143-x

Kabanda TA, Jury MR (1999) Inter-annual variability of short rains over northern Tanzania. Clim Res 13:231–241

Liebmann B, Hoerling MP, Funk C, Bladé I, Dole RM, Allured D, Quan X, Pegion P, Eischeid JK (2014) Understanding recent eastern Horn of Africa rainfall variability and change. J Clim 27:8630–8645. https://doi.org/10.1175/JCLI-D-13-00714.1

Lloyd-Hughes B (2012) A spatio-temporal structure-based approach to drought characterisation. Int J Climatol 32:406–418. https://doi.org/10.1002/joc.2280

Lukamba MT (2010) Natural disasters in African countries: what can we learn about them? TD J Transdiscipl Res South Afr 6:478–495. https://doi.org/10.4102/td.v6i2.266

Lyon B, DeWitt DG (2012) A recent and abrupt decline in the East African long rains. Geophys Res Lett 39:L02702. https://doi.org/10.1029/2011GL050337

Maidment RI, Allan RP, Black E (2015) Recent observed and simulated changes in precipitation over Africa. Geophys Res Lett 42:8155–8164. https://doi.org/10.1002/2015GL065765

Makula EK, Zhou B (2021) CMIP6 evaluation and projection of East African Precipitation. Int J Climatol. https://doi.org/10.1002/joc.7207

Maraun D (2013) Bias correction, quantile mapping, and downscaling: revisiting the inflation issue. J Clim 26:2137–2143. https://doi.org/10.1175/JCLI-D-12-00821.1

Martey E, Etwire PM, Kuwornu JKM (2020) Economic impacts of smallholder farmers' adoption of drought-tolerant maize varieties. Land Use Policy 94:104524. https://doi.org/10.1016/j.landusepol.2020.104524

Masih I, Maskey S, Mussá FEF, Trambauer P (2014) A review of droughts on the African continent: a geospatial and long-term perspective. Hydrol Earth Syst Sci 18:3635–3649. https://doi.org/10.1016/j.jhydrol.2010.07.012

McKee TB, Doesken NJ, Kleist J (1993) The relationship of drought frequency and duration to time scales. In: Proc 8th Conf Appl Climatol 17: 179–183

Meehl GA, Covey C, Delworth T, Latif M, McAvaney B, Mitchell JFB, Stouffer RJ, Taylor KE (2007) The WCRP CMIP3 multimodel dataset: a new era in climate change research. Bull Am Meteorol Soc 88:1383–1394. https://doi.org/10.1175/BAMS-88-9-1383

Mishra AK, Singh VP (2010) A review of drought concepts. J Hydrol 39:202–216. https://doi.org/10.1016/j.jhydrol.2010.07.012

Mondal SK, Huang J, Wang Y et al (2021) Doubling of the population exposed to drought over South Asia: CMIP6 multi-model-based analysis. Sci Total Environ 771:145186. https://doi.org/10.1016/j.scitotenv.2021.145186

Ngoma H, Wen W, Ayugi B, Babaousmail H, Karim R, Ongoma V (2021) Evaluation of rainfall simulations in CMIP6 models over Uganda. Int J Climatol 41:4743–4768. https://doi.org/10.1002/joc.7098

Nguvava M, Abiodun BJ, Otieno F (2019) Projecting drought characteristics over East African basins at specific global warming levels. Atmos Res 228:41–54. https://doi.org/10.1016/j.atmosres.2019.05.008

Nicholson SE (2017) Climate and climatic variability of rainfall over eastern Africa. Rev Geophys 55:590–635. https://doi.org/10.1002/2016RG000544

Nicholson SE (2018) The ITCZ and the seasonal cycle over equatorial Africa. Bull Am Meteorol Soc 99:337–348. https://doi.org/10.1175/BAMS-D-16-0287.1

Nkunzimana A, Shuoben B, Guojie W, Alriah MAA, Sarfo I, Zhihui X, Vuguziga F, Ayugi BO (2021) Assessment of drought events, their trend and teleconnection factors over Burundi, East Africa. Theor Appl Climatol 145:1293–1316. https://doi.org/10.1007/s00704-021-03680-3

Ntale HK, Gan TY (2003) Drought indices and their application to East Africa. Int J Climatol 23:1335–1357. https://doi.org/10.1002/joc.931

Ntiba MJ, Kudoja WM, Mukasa CT (2001) Management issues in the Lake Victoria watershed. Lakes Reserv: Res Manag 6:211–216. https://doi.org/10.1046/j.1440-1770.2001.00149.x

O'Neill BC, Kriegler E, Ebi KL, Kemp-Benedict E, Riahi K, Rothman DS, van Ruijven BJ, van Vuuren DP, Birkmann J, Kok K (2017) The roads ahead: Narratives for shared socioeconomic pathways describing world futures in the 21st century. Glob Environ Chang 42:169–180. https://doi.org/10.1016/j.gloenvcha.2015.01.004

Ogwang BA, Chen H, Li X, Gao C (2014) The influence of topography on East African October to December climate: sensitivity experiments with RegCM4. Adv Meteorol 2014:143917. https://doi.org/10.1155/2014/143917

Ogwang BA, Ongoma V, Xing L, Ogou KF (2015) Influence of mascarene high and Indian Ocean dipole on East African extreme weather events. Geogr Pannonica 19:64–72

Omondi PA, Awange JL, Forootan E et al (2014) Changes in temperature and precipitation extremes over the greater Horn of Africa region from 1961 to 2010. Int J Climatol 34:1262–1277. https://doi.org/10.1002/joc.3763

Ongoma V, Chen H (2017) Temporal and spatial variability of temperature and precipitation over East Africa from 1951 to 2010. Meteorol Atmos Phys 129:131–144. https://doi.org/10.1007/s00703-016-0462-0

Ongoma V, Tan G, Ogwang B, Ngarukiyimana J (2015) Diagnosis of seasonal rainfall variability over East Africa: a case study of 2010–2011 drought over Kenya. Pakistan J Meteorol 11:13–21

Ongoma V, Chen H, Gao C, Nyongesa AM, Polong F (2018a) Future changes in climate extremes over equatorial East Africa based on CMIP5 multimodel ensemble. Nat Hazards 90:901–920. https://doi.org/10.1007/s11069-017-3079-9

Ongoma V, Chen H, Gao C (2018b) Projected changes in mean rainfall and temperature over East Africa based on CMIP5 models. Int J Climatol 38:1375–1392. https://doi.org/10.1002/joc.5252

Ongoma V, Chen H, Omony GW (2018c) Variability of extreme weather events over the equatorial East Africa, a case study of rainfall in Kenya and Uganda. Theor Appl Climatol 131:295–308. https://doi.org/10.1007/s00704-016-1973-9

Ongoma V, Chen H, Gao C, Sagero PO (2018d) Variability of temperature properties over Kenya based on observed and reanalyzed datasets. Theor Appl Climatol 133:1175–1190. https://doi.org/10.1007/s00704-017-2246-y

Onyutha C, Asiimwe A, Ayugi B, Ngoma H, Ongoma V, Tabari H (2021) Observed and future precipitation and evapotranspiration in water management zones of Uganda: CMIP6 projections. Atmosphere 12(7):887. https://doi.org/10.3390/atmos12070887

Opiyo F, Wasonga O, Nyangito M, Schilling J, Munang R (2015) Drought adaptation and coping strategies among the Turkana pastoralists of northern Kenya. Int J Disaster Risk Sci 6:295–309. https://doi.org/10.1007/s13753-015-0063-4

Ostad-Ali-Askari K, Ghorbanizadeh Kharazi H, Shayannejad M, Zareian MJ (2019) Effect of management strategies on reducing negative impacts of climate change on water resources of the Isfahan-Borkhar aquifer using MODFLOW. River Res Applic 35:611–631. https://doi.org/10.1002/rra.3463

Osuch M, Romanowicz RJ, Lawrence D, Wong WK (2016) Trends in projections of standardized precipitation indices in a future climate in Poland. Hydrol Earth Syst Sci 20:1947–1969. https://doi.org/10.5194/hess-20-1947-2016

Otieno HO, Awange JL (2006) Energy resources in East Africa: Opportunities and challenges. Springer-Verlag, Heidelberg

Peel MC, Finlayson BL, Mcmahon TA (2007) Updated world map of the Koppen-Geiger climate classification. Hydrol Earth Syst Sci 11:1633–1644. https://doi.org/10.5194/hess-11-1633-2007

Phillips CA, Caldas A, Cleetus R, Dahl KA et al (2020) Compound climate risks in the COVID-19 pandemic. Nat Clim Chang 10:586–588. https://doi.org/10.1038/s41558-020-0804-2

Piani C, Haerter JO, Coppola E (2010) Statistical bias correction for daily precipitation in regional climate models over Europe. Theor Appl Climatol 99:187–192. https://doi.org/10.1007/s00704-009-0134-9

Sagero PO, Shisanya CA, Makokha GL (2018) Investigation of rainfall variability over Kenya (1950–2012). J Environ Agric Sci 14:1–15

Schneider U, Becker A, Finger P, Meyer-Christoffer A, Rudolf B, Ziese M (2015) GPCC full data reanalysis version 7.0 (at 0.5°, 1.0°, 2.5°): Monthly Land-Surface Precipitation from Rain-Gauges built on GTS-based and Historic Data. https://doi.org/10.5676/DWD_GPCC/FD_M_V7_050

Sheffield J, Wood EF, Roderick ML (2012) Little change in global drought over the past 60 years. Nature 491:435–438. https://doi.org/10.1038/nature11575

Sheffield J, Wood EF (2007) Projected changes in drought occurrence under future global warming from multi-model, multi-scenario, IPCC AR4 simulations. Clim Dyn 31(1):79–105. https://doi.org/10.1007/s00382-007-0340-z

Shongwe ME, van Oldenborgh GJ, van den Hurk B, van Aalst M (2011) Projected changes in mean and extreme precipitation in Africa under global warming. Part II: East Afr J Clim 24:3718–3733. https://doi.org/10.1175/2010JCLI2883.1

Shrestha A, Rahaman MM, Kalra A, Jogineedi R, Maheshwari P (2020) Climatological drought forecasting using bias corrected CMIP6 climate data: a case study for India. Forecasting 2:59–84. https://doi.org/10.3390/forecast2020004

Song Y, Semazzi FHM, Xie L, Ogallo LJ (2004) A coupled regional climate model for the Lake Victoria basin of East Africa. Int J Climatol 24:57–75. https://doi.org/10.1002/joc.983

Spinoni J, Barbosa P, Bucchignani E et al (2020) Future global meteorological drought hot spots: a study based on CORDEX data. J Clim 33:3635–3661. https://doi.org/10.1175/JCLI-D-19-0084.1

Steffen W, Rockström J, Richardson K et al (2018) Trajectories of the earth system in the anthropocene. Proc Natl Acad Sci USA 115:8252–8259. https://doi.org/10.1073/pnas.1810141115

Swann ALS, Hoffman FM, Koven CD, Randerson JT (2016) Plant responses to increasing $CO_2$ reduce estimates of climate impacts on drought severity. Proc Natl Acad Sci 113:10019–10024. https://doi.org/10.1073/pnas.1604581113

Tabari H, Paz SM, Buekenhout D, Willems P (2021) Comparison of statistical downscaling methods for climate change impact analysis on precipitation-driven drought. Hydrol Earth Syst Sci 25:3493–3517. https://doi.org/10.5194/hess-25-3493-2021

Tan G, Ayugi B, Ngoma H, Ongoma V (2020) Projections of future meteorological drought events under representative concentration pathways (RCPs) of CMIP5 over Kenya. East Africa Atmos Res 246:105112. https://doi.org/10.1016/j.atmosres.2020.105112

Tayler KE, Stouffer RJ, Meehl GA (2012) An overview of CMIP5 and the experimental design. Bull Am Meteorol Soc 93:485–498. https://doi.org/10.1175/BAMS-D-11-00094.1

Tian B, Dong X (2020) The Double-ITCZ bias in CMIP3, CMIP5, and CMIP6 models based on annual mean precipitation. Geophys Res Lett. https://doi.org/10.1029/2020GL087232

Trenberth KE (2011) Changes in precipitation with climate change. Clim Res 47:123–138. https://doi.org/10.3354/cr00953

Trenberth KE, Dai A, Van Der Schrier G et al (2014) Global warming and changes in drought. Nat Clim Chang 4:17–22. https://doi.org/10.1038/nclimate20167

Trisos CH, Adelekan IO, Totin E, et al. (2022) Africa In: Climate Change 2022: Impacts, Adaptation, and Vulnerability. Contribution of Working Group II to the Sixth Assessment Report of the Intergovernmental Panel on Climate Change. In: Pörtner H-O, Roberts DC, Tignor M, et al. (Eds.), Cambridge University Press, Cambridge

Ukkola AM, Pitman AJ, De Kauwe MG et al (2018) Evaluating CMIP5 model agreement for multiple drought metrics. J Hydrometeorol 19:969–988. https://doi.org/10.1175/JHM-D-17-0099.1

Ukkola AM, De Kauwe MG, Roderick ML, Abramowitz G, Pitman AJ (2020) robust future changes in meteorological drought in CMIP6 projections despite uncertainty in precipitation. Geophy Res Lett. https://doi.org/10.1029/2020GL087820

van Dijk AIJM, Beck HE et al (2013) The Millennium Drought in southeast Australia (2001–2009): Natural and human causes and implications for water resources, ecosystems, economy, and society. Water Resour Res 49:1040–1057. https://doi.org/10.1002/wrcr.20123

Wang Z, Zhong R, Lai C, Zeng Z, Lian Y, Bai X (2018) Climate change enhances the severity and variability of drought in the Pearl River Basin in South China in the 21st century. Agric Meteorol 249:149–162. https://doi.org/10.1016/j.agrformet.2017.12.077

Wei Y, Yu H, Huang J, Zhou T, Zhang M, Ren Y (2019) Drylands climate response to transient and stabilized 2 °C and 1.5 °C global warming targets. Clim Dyn 53:2375–2389. https://doi.org/10.1007/s00382-019-04860-8

Wilhite DA, Svoboda MD (2000) Drought early warning systems in the context of drought preparedness and mitigation. Early Warn. Syst. Drought Prep. Drought Manag. Accessed 10, Sep 2021 https://www.unisdr.org/files/1882_VL102149.pdf

Wu H, Hayes MJ, Wilhite DA, Svoboda MD (2005) The effect of the length of record on the standardized precipitation index calculation. Int J Climatol 25:505–520. https://doi.org/10.1002/joc.1142

Yang T, Ding J, Liu D, Wang X, Wang T (2019) Combined use of multiple drought indices for global assessment of dry gets drier and wet gets wetter paradigm. J Clim 32:737–748. https://doi.org/10.1175/JCLI-D-18-0261.1

Zhai L, Feng Q (2009) Spatial and temporal pattern of precipitation and drought in Gansu Province, Northwest China. Nat Hazards 49:1–24. https://doi.org/10.1007/s11069-008-9274-y

Zhai J, Mondal SK, Fischer T et al (2020) Future drought characteristics through a multi-model ensemble from CMIP6 over South Asia. Atmos Res 246:105111. https://doi.org/10.1016/j.atmosres.2020.105111

Zhao JT, Da SuB, Mondal SK, Wang YJ, Tao H, Jiang T (2021) Population exposure to precipitation extremes in the Indus River Basin at 1.5°C, 2.0°C and 3.0°C warming levels. Adv Clim Chang Res 12:199–209. https://doi.org/10.1016/j.accre.2021.03.005



## Authors and Affiliations

**Brian Ayugi[1,2] · Zablon Weku Shilenje[3,4] · Hassen Babaousmail[5] · Kenny T. C. Lim Kam Sian[5] · Richard Mumo[6] · Victor Nnamdi Dike[7,8] · Vedaste Iyakaremye[2,9] · Abdelghani Chehbouni[10] · Victor Ongoma[10]**

1 Jiangsu Key Laboratory of Atmospheric Environment Monitoring and Pollution Control, Collaborative Innovation Center of Atmospheric Environment and Equipment Technology, School of Environmental Science and Engineering, Nanjing University of Information Science and Technology, Nanjing 210044, China

2 Key Laboratory of Meteorological Disaster, Ministry of Education (KLME), Joint International Research Laboratory of Climate and Environment Change (ILCEC)/Collaborative Innovation Center On Forecast and Evaluation of Meteorological Disasters (CIC-FEMD), University of Information Science and Technology, NanjingNanjing 210044, China

3 Department of Atmospheric Physics, Faculty of Mathematics and Physics, Charles University, 18000 Praha 8, Prague, Czech Republic

4 Kenya Meteorological Department, P.O. Box 30259-00100, Nairobi, Kenya

5 Binjiang College of Nanjing University of Information Science and Technology, Wuxi 214105, China

6 Department of Mathematics and Statistical Sciences, Botswana International University of Science and Technology, Plot 10071, Private Bag 16, Palapye, Botswana

[7] International Center for Climate and Environment Sciences, Institute of Atmospheric Physics, Chinese Academy of Sciences, Beijing 100029, China

[8] Energy, Climate, and Environment Science Group, Imo State Polytechnic Umuagwo, Ohaji, PMB, Owerri 1472, Imo State, Nigeria

[9] Rwanda Meteorology Agency, Nyarugenge KN 96 St, Kigali, Rwanda

[10] International Water Research Institute, Mohammed VI Polytechnic University, Lot 660, Hay Moulay Rachid, 43150 Ben Guerir, Morocco